Century scale trends and seasonality in pH and temperature for shallow zones of the Bering Sea

Jan Fietzke[a,1], Federica Ragazzola[a,b,c], Jochen Halfar[d], Heiner Dietze[a], Laura C. Foster[b], Thor H. Hansteen[a], Anton Eisenhauer[a], and Robert S. Steneck[e]

[a]GEOMAR Helmholtz Centre for Ocean Research Kiel, Wischhofstr. 1-3, 24148 Kiel, Germany. [b]Dept. of Earth Sciences, Univ. of Bristol, Wills Memorial Building, Queen´s Road, BS8 1RJ, Bristol, UK. [c]Institute of Marine Sciences, Univ. of Portsmouth, Langstone Harbour, Ferry Road, Eastney, Portsmouth, P04 9LY, UK. [d]Dept. of Earth Sciences, Univ. of Toronto, Mississauga, ON L5L 1C6, Canada. [e]School of Marine Sciences, Univ. of Maine, Darling Marine Center, 193 Clarks Cove Rd, Walpole, ME 04573, USA. [1]Corresponding author: jfietzke@geomar.de

Submitted to Proceedings of the National Academy of Sciences of the United States of America

No records exist to evaluate long-term pH dynamics in high-latitude oceans, which have the greatest probability of rapid acidification from anthropogenic CO2 emissions. We reconstructed both seasonal variability and anthropogenic change in seawater pH and temperature by using laser ablation high-resolution 2D images of stable boron isotopes (δ11B) on a long-lived coralline alga that grew continuously through the 20th century. Analyses focused on four multi-annual growth segments. We show a long-term decline of 0.08±0.01 pH units between the end of the 19th and 20th century which is consistent with atmospheric CO2 records. Additionally, a strong seasonal cycle (~0.22 pH units) is observed and interpreted as episodic annual pH increases caused by the consumption of CO2 during strong algal (kelp) growth in spring and summer. The rate of acidification intensifies from -0.006±0.007 pH units per decade (between 1920's and 1960's) to -0.019±0.009 pH units per decade (between 1960's and 1990's) while the episodic pH increases show a continuous shift to earlier times of the year throughout the centennial record. This is indicative of ecosystem shifts in shallow water algal productivity in this high-latitude habitat resulting from warming and acidification.

ocean acidification | boron isotopes | isotope imaging | laser ablation ICP-MS | crustose algae

So far about 30 % of the anthropogenic carbon dioxide emissions have been taken up by the oceans (*1, 2*) which are one of the major reservoirs of the global carbon cycle. Since the mid-19th century the carbon dioxide concentration in the atmosphere has increased to more than 390 µatm (*3*), well above the typical range reconstructed for the glacial/interglacial cycles (190-280 µatm) over the last 500,000 yrs. This increase in atmospheric CO_2 has shifted the carbonic acid equilibrium in seawater, resulting in a pH decrease (ocean acidification) lowering the carbonate ion concentration. Over the last ~150 years the global average surface water pH has declined by about 0.15 pH units (*2*) and is expected to have further decreased by 0.3-0.4 pH units by the year 2100 (*4*). This is expected to trigger major shifts in marine ecosystems, challenging marine calcifiers' ability to form carbonate hard substrate as a consequence of a lowered calcium carbonate saturation state (*4-6*). This reduction of saturation (i.e. increase in solubility) is a direct consequence of the lowered carbonate ion concentration. Compared to this the weak increase in saturation from rising temperatures (ocean warming) is almost negligible (*7*). Recent research on future changes of marine ecosystems has largely focused on laboratory-based culturing studies and mesocosm experiments (*6, 8, 9*). However, to make realistic predictions additional information about past natural variability also needs to be obtained directly from long-lived calcifiers, which experienced a whole complexity of challenges within their natural habitats including pH variability (*10*).

Proxy-based reconstructions of ocean pH are commonly made by mass spectrometric determination (TIMS, SIMS and MC-ICP-MS) of $\delta^{11}B$ on discrete carbonate samples (*11-14*). Using these methods long-term records of ocean pH variability have been established (*15-17*). However, these time-series suffer from poor temporal resolution and do not resolve small-scale spatial heterogeneities of natural samples. High-resolution records are desired since they allow for investigation of both, short-term variability and long-term trends in pH. Furthermore, available pH proxy-records focus on the tropics. At high latitudes no such data are available, despite the fact that these regions naturally show low carbonate saturation state and the highest CO_2 uptake due to the cold surface water temperature.

For the first time we apply the recently developed Laser-Ablation-Multi-Collector-ICP-MS (LA-MC-ICP-MS) in-situ method (*18*) as a microchemical imaging technique to provide a spatially and temporally highly resolved $\delta^{11}B$ record from a long-lived subarctic coralline alga. Crustose coralline red algae are long-lived marine organisms that form annually laminated high-Mg-calcite structures (*19*). They are among the major calcifiers in shallow-water benthic communities from the tropics to polar regions (*20, 21*). The chemical composition of their skeleton is controlled by algal physiology responding to the environmental parameters (e.g. light, nutrients, temperature, pH) (*22, 23*). Coralline algae have received widespread attention as temperature proxy archives on weekly to multi-centennial timescales (*19, 24, 25*).

For this study we used a sample (Figure 1) of the alga *Clathromorphum nereostratum* Lebednik, collected alive at 10

Significance

Increasing atmospheric CO2 concentrations are potentially affecting marine ecosystems twofold, by warming and acidification. The rising amount of CO2 taken up by the ocean lowers the saturation state of calcium carbonate complicating the formation of this key biomineral utilized by many marine organisms to build hard parts like skeletons or shells. Reliable time-series data of seawater pH are needed to evaluate the ongoing change and compare long-term trends and natural variability. For the high-latitude ocean, the region facing the strongest CO2 uptake, such time-series data are so far entirely lacking. Our study provides the first reconstruction of seasonal cycle and long-term trend in pH for a high-latitude ocean obtained from 2D images of stable boron isotopes from a coralline alga.

Reserved for Publication Footnotes

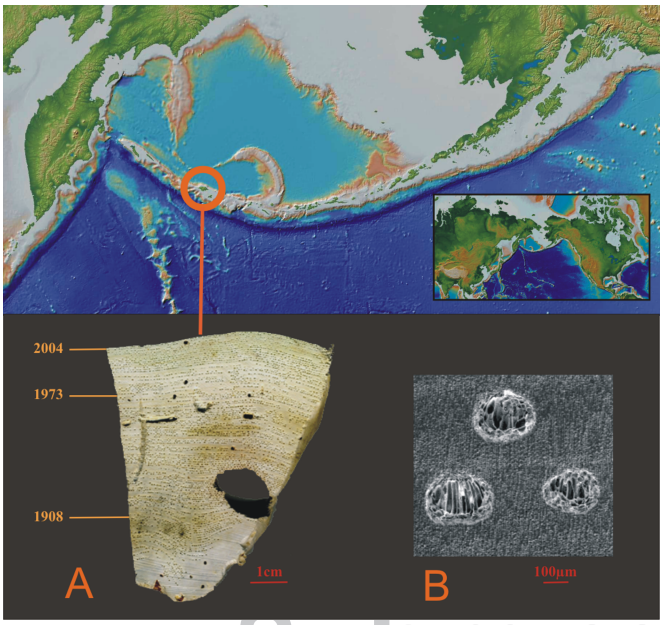

Fig. 1. ***Clathromorphum nereostratum*** **sample from Attu Island, Alaska.** A) Overview image of the sample including reference dates (*29*), lines of dark spots are conceptacle cavities. B) Secondary Electron (SE) image of reproductive structures (conceptacles).

m water depth off the eastern coast of Attu Island (Massacre Bay at Murder Point, Attu, Aleutian Islands – N 52° 47.787, E 173° 10.796) in August 2004. The local habitat is ecologically dominated by an annually growing kelp species (Dragon kelp, *Eualaria fistulosa*) being the main primary producer. The coastal waters of Attu Island are free of ice the whole year round (annual SST range: 2.2 - 10.5 °C, based on ERSST v2 (*26*)). The steep slopes of the Aleutian Island chain create a dynamic oceanographic environment (including upwelling) featuring the Alaskan Stream as the main current system south of the islands. This strong, westward boundary current transports relatively warm nutrient-rich low salinity (~32 psu) water passing through the gaps between the Aleutian Islands. It forms the Aleutian North Slope Current (ANSC), an eastward current north of the island chain. One of the main inflows of the Alaskan Stream into the Bering Sea is Near Strait, located west of Attu Island (*27, 28*). The influence of the Pacific Decadal Oscillation (PDO) on the multi-decadal climate variability at the collection site has been reported in a previous publication (*29*).

The collected *C. nereostratum* specimen revealed a continuous growth record spanning from 1887 to 2004 (Figure 1A) with growth rate averaging 370 µm/y (*29*). The age model has previously been established by counting annual growth increments and validated by U/Th dates (*29*). The visual identification of annual growth increments is additionally aided by the annual formation of conceptacle cavities (reproductive structures; Figure 1B). Starting in late summer conceptacles develop in cavities partially formed by dissolution of the formerly precipitated calcite skeleton (*30*). The newly formed calcite structures within and surrounding the conceptacles may contain re-precipitated material and are morphologically and chemically distinct from the primary calcite. Hence, reliable proxy data can only be obtained from the primary calcite found in the vegetative thallus.

Mg/Ca ratios in different coralline algal species have previously been shown to be positively related to ambient seawater temperatures (*24, 25, 31, 32*). Mg/Ca based temperature time series obtained from Mg/Ca electron microprobe (EMP) elemental mappings display a characteristic pattern related to the seasonal cycle in ambient water temperature (spatially biased by variable algal growth rates). Minima of 2-3 °C during winter and maxima of 10-11 °C mark the annual cycle recorded by the algal skeleton (Figure 2). Element maps indicate that about 75 % of the annually precipitated calcite is related to spring and summer growth. The growth rate declines significantly by the end of summer. A likely explanation for this growth rate reduction is the beginning of conceptacle formation by the end of summer, as insolation declines and algal physiology shifts from growth to reproduction. It is also apparent from the elemental maps that conceptacle calcite contains significantly higher amounts of Mg than primary calcite and therefore must be excluded from the temperature reconstruction. Mean temperatures derived from Mg/Ca maps (see Figure 2) of 5.3 °C (M-1887/97; for sample denotation see methods) and 6.2 °C (M-1987/96) suggest a warming trend over the 100 year period.

Within the areas used for high resolution EMP analysis we acquired the first accurate and precise 2D images representing the variability of stable isotopes of boron ($^{11}B/^{10}B$) in natural samples using LA-MC-ICP-MS (*18*) at a resolution of 100 µm. This allows for the visualization of the spatial distribution of isotopic signatures in a complex sample (Figure 3A, see supporting information for methods). In addition to cyclic intra-annual $\delta^{11}B$ variability, the distinct composition of conceptacle calcite is apparent in the $\delta^{11}B$ images. This further highlights differences in the calcification process of both, primary and secondary calcite.

C. nereostratum shows a large degree of variability in $\delta^{11}B$ values ranging from about 21-27. The low values are clearly associated with conceptacle areas (Figure 3A). Using only data from primary calcite (see supporting information) $\delta^{11}B$ averages in B-1888/94 are by about 1 to 1.2 higher than in B-1989/96. The conversion of $\delta^{11}B$ into pH revealed a decline of 0.08±0.01 pH units between B-1888/94 and B-1989/96, while the absolute boron-derived pH values are almost 0.7 pH units above the reasonable ambient seawater pH range in the Bering Sea. A comparable offset between $\delta^{11}B$-derived and ambient seawater pH has also been observed in other marine calcifying organisms e.g. corals (*33-36*). It is interpreted as the result of the organism's physiological control on the calcifying fluid composition, up-regulating the pH relative to ambient seawater to provide more alkaline conditions to promote calcification (*33-36*). $\delta^{11}B$ is considered to represent the calcifying fluid pH (pH_{cf}). For corals $\delta^{11}B$-pH calibration studies revealed the up-regulation being species-dependent resulting in an approximately half as strong change in pH_{cf} relative to the external pH change (*34*). Nevertheless, different coral species show distinct sensitivities in the response to acidification and, thus, differ in their $\delta^{11}B$-pH relationship, i.e. their up-regulation potential (*33, 34*).

No $\delta^{11}B$-pH calibration studies exist for coralline algae so far. Future studies will reveal if or to what extend the mentioned systematic found for corals can be transferred to coralline algae. A recently published study suggests the impact of seawater chemistry on the calcification is more direct for coralline algae than for corals (*37*). Consequently, we reconstruct pH_{cf} and its temporal changes from $\delta^{11}B$ in our algal sample. The observed drop of 0.08±0.01 pH units is in good agreement with the expected shift in sea surface water pH from rising atmospheric pCO_2 levels (1900: ~295 µatm; 1990´s: ~360 µatm). This suggests that boron isotope data derived from *C. nereostratum* accurately reflect long-term changes in sea water pH. It also implies the pH_{cf} in this algal species follows external pH more closely than reported for corals. Despite the long-term pH decline recorded by the coralline alga, potential negative impacts on annual skeletal growth rates of Bering Sea *C. nereostratum* corallines have not yet been observed (*19*).

Furthermore, the $\delta^{11}B$ images reveal cyclic variations (Figure 3B), pointing to a distinct seasonal cycle of pH_{cf} and consequently

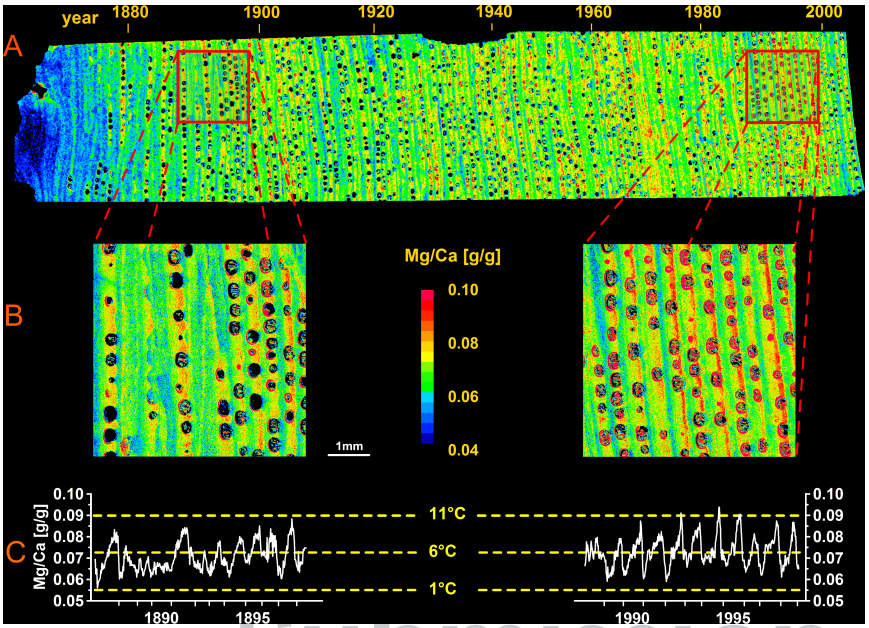

Fig. 2. Electron microprobe Mg/Ca elemental ratio maps used for temperature reconstruction. A) Overview map of the whole sample (30 µm resolution) to examine long-term variability in Mg/Ca. B) Subsample maps (5 µm resolution) from early-industrial (M-1887/97) and recent (M-1988/98) to examine intra-annual variability in Mg/Ca. "M-years" designates the respective EMP map and the time interval covered. C) Temperature reconstructed from Mg/Ca using data from B). Each data point of the time series represents average values of about 100 individual Mg/Ca data points from the original mappings (see supporting information for data treatment).

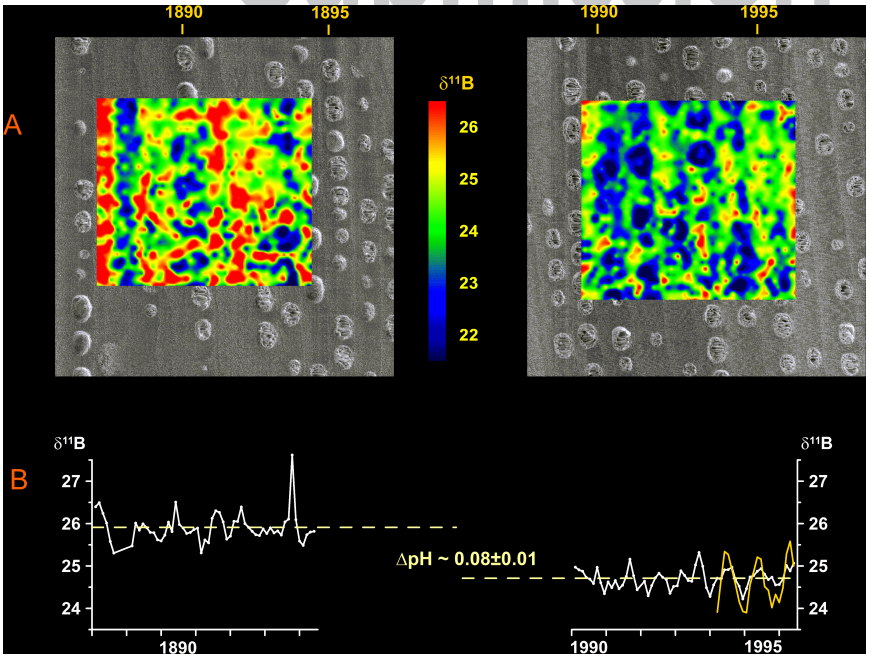

Fig. 3. Stable boron isotope ratio ($\delta^{11}B$) images acquired by LA- MC-ICP-MS used for pH reconstruction. A) $\delta^{11}B$ images (100 µm resolution) displayed as overlays on secondary electron images from the electron microprobe measurements (Fig. 2) referred to as B-1888/1894 and B-1989/96 in the text. B) $\delta^{11}B$ time series showing a long-term decrease equal to 0.08±0.01 pH units between the 1890's and 1990's in good agreement with atmospheric CO_2 records (see text and supplementary material). Additionally, a seasonal pH cycle of at least 0.1 pH units can be seen for the years 1994-1996 (*yellow*) using only data from the area least influenced by secondary calcite (see supporting information for data treatment).

seawater pH. When comparing the spatial distribution of both $\delta^{11}B$ and Mg/Ca maps we find the highest boron isotopic values clearly preceding the annual peak in Mg/Ca. This suggests that the pH maximum occurs during late spring/early summer growth intervals (see supporting information S4). This seasonal cycle in $\delta^{11}B$ of up to 5 is observed for all 14 annual growth layers investigated in TS-1923/27, TS-1961/65 and TS-1989/92 (Figure 4D). Less than 30% of the variability in $\delta^{11}B$ results from the influence of temperature on the boric acid pK_B. The remaining signal trend corresponds to an average intra-annual pH_{cf} variability of 0.22±0.03 with the lowest values during winter and early spring and maxima during late spring and summer.

How does the observed algal annual pH data compare to what is known for the region? Attu Island is uninhabited and no time-series pH data have been made available to date. Hence, we are restricted to gridded climatological data. Using a recently published global seawater carbonate system dataset (*38*) we can estimate an annual pH signal for the open waters around Attu in the order of about 0.1 pH units (see details in supporting information S5, Fig. S8), lowest pH calculated for January-March and highest values for July-October. This signal is less than half of what we have reconstructed from $\delta^{11}B$ in our algal sample. However, a significantly larger variability in pH is possible for the local coastal habitat where our *C. nereostratum* specimen had grown. As mentioned above the local habitat is dominated by annually growing kelp, being the dominant primary producer. Kelp-dominated habitats are reported to be among the most productive ecosystems in the global ocean (*39, 40*). Starting in spring these

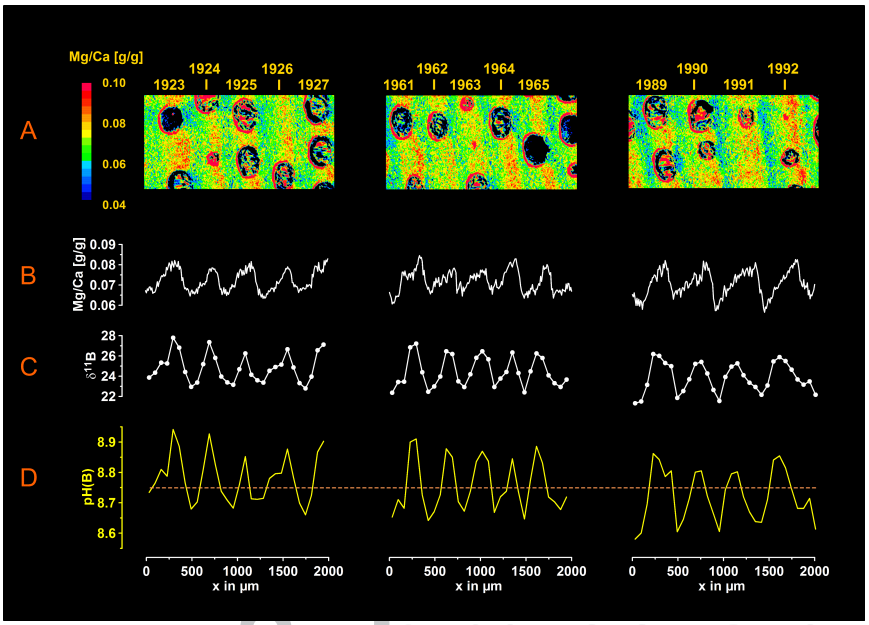

Fig. 4. Seasonal pH variability. A) EMP Mg/Ca elemental maps (10 µm resolution) for the time slices (TS-1923/27, TS-1961/65, TS-1989/92) selected for not showing any traces of skeletal destruction from grazing. "TS-years" designates the $\delta^{11}B$ time series and the time interval covered. B) Mg/Ca time series' obtained from a) used for temperature calculation. C) $\delta^{11}B$ time series determined via LA-MC-ICP-MS (66µm resolution). D) internal (calcifying fluid) pH derived from $\delta^{11}B$ time series using Mg/Ca derived temperatures to correct boric acid pK_B (for details see text and supporting information). Dashed line represents the mean pH (8.75) of the three time series data.

fast-growing macro algae consume huge amounts of CO_2 for photosynthesis. As a consequence of depletion in dissolved CO_2 in the water the carbonic acid equilibrium should shift towards higher pH values. Indeed, highly dynamic pH conditions have been reported for kelp-dominated habitats (*41*). Our observation of pH maxima occurring in spring/ early summer agrees with the seasonality of kelp growth in this habitat supporting the proposed effect.

Further support for the assumed higher pH dynamic linked to enhanced productivity is provided by the oceanographic environment, local topography and remote-sensing data. As pointed out before strong currents (Alaskan Stream in the South and Aleutian North Slope Current in the North) including the northward inflow into the Bering Sea through Near Strait are the prominent hydrographic features close to Attu Island. The steep island slopes foster upwelling of nutrient-rich deeper water masses. A resulting enhanced productivity in coastal waters (so-called "island mass effect") has been reported for comparable environmental settings (*42, 43*). Satellite data of Chlorophyll a provide clear evidence for Attu Island being a productivity hotspot (for details see supporting information S5, Fig. S9). During summer Chlorophyll a concentrations in coastal waters south-east off Attu Island exceed 2 mg/m^3 while in open waters of this region 0.2-0.6 mg/m^3 is measured.

We therefore think a larger annual pH cycle than suggested by climatological data for open waters can be expected for this coastal habitat and is recorded by $\delta^{11}B$ in the calcite skeleton of *C. nereostratum*. Ultimately, $\delta^{11}B$-pH calibration studies are needed using specimens cultured under controlled conditions or free-living ones after data logger had been deployed in the natural habitat. For now winter/early spring growth layers, when ambient water pCO_2 is equilibrated with the atmosphere (equating to $\delta^{11}B$ minima), are considered the most useful to assess the long-term pH trend. Indeed we find a gradual decline for the average internal pH minima (TS-1923/27: 8.683±0.021; TS-1961/65: 8.660±0.015; TS-1989/92: 8.608±0.020). This trend agrees well with the centennial 0.08±0.01 reduction in pH obtained from B-1888/94 and B-1989/96 (Fig. 4D). Our results indicate an increase in the rate of acidification from -0.006±0.007 pH units per decade (between 1920's and 1960's) to -0.019±0.009 pH units per decade (between 1960's and 1990's) closely following the trend in atmospheric CO_2 concentration. With respect to relative pH change our findings agree with the estimated global average surface water pH decline of 0.15 pH units over the last ~150 years *(2)*. Nevertheless, due to the low water temperatures in this high latitude ocean habitat calcium carbonate saturation is significantly lower than in the tropical or temperate regions of the global oceans. Thus, any further saturation state reduction from lowered pH will potentially affect calcifying organisms stronger in the habitat investigated. Our results, however, are based on the four growth segments analyzed. Therefore, we cannot rule out inter-annual or inter-decadal pH variability which future studies should focus on.

The comparison of annual Mg/Ca and $\delta^{11}B$ peak positions in the time series data provides a first indication of long-term temporal shifts of algal (kelp) growth season (see supporting information S6). Mg/Ca peaks, indicating the annual temperature maxima, show a weak temporal trend towards higher relative positions within the annual growth band, possibly due to an increase in spring/summer growth. An opposite trend towards lower relative positions is observed for $\delta^{11}B$ peaks representing pH which always precede their corresponding Mg/Ca peak. The offset between $\delta^{11}B$ and Mg/Ca peaks (expressed as % of annual growth) changed from 10±9 % (TS-1923/27) to 20±11 % (TS-1961/65) and 39±10 % (TS-1989/92). This is interpreted as a long-term shift of algal (kelp) growth towards earlier times of the season in the study area. Together with the above mentioned warming trend our results indicate an ongoing ecosystem shift in this high-latitude ocean coastal habitat.

The detection of intra-annual variability in pH caused by the seasonal uptake of CO_2 by algae (kelp) for photosynthesis applying the presented methodology enables us to reconstruct intensities and timing of the growth season influenced by parameters like light, temperature, nutrient supply (e.g. from upwelling or volcanic ash supply) over wide temporal and spatial scales. Particularly, through the use of long-lived crustose coralline algae natural pH variability and long-term trends can be investigated in the higher latitudes, the part of the oceans showing the strongest CO_2 uptake. In combination with similar records from lower latitudes e.g. using corals or coralline algae this will help to increase our understanding of the complex responses of marine

ecosystems with respect to pH in a world of further increasing atmospheric CO_2.

Methods

Stable boron isotope analysis via LA-MC-ICP-MS was performed using two different approaches (for full technical details see supporting information S3):

1) 2D images (3x3 mm², 100 µm resolution) referred to as boron images B-1888/94 and B-1989/96 were acquired to evaluate the spatial distribution of $\delta^{11}B$. The growth periods covered are B-1889/94: 1888-1894 and B-1989/96: 1989-1996 (Figure 3A).

2) Time series (2 mm long, 66 µm resolution) focussing on primary calcite to evaluate the intra-annual variability of $\delta^{11}B$ and to put better constraints on the long-term trend observed between B-1889/94 and B-1989/96 (see main text). Three time series have been acquired for the years 1923-1927 (TS-1923/27), 1961-1965 (TS-1961/65) and 1989-1992 (TS-1989/92) (Figure 4C).

In order to identify representative regions for LA-MC-ICP-MS boron measurements calibrated Mg/Ca elemental maps were generated using electron microprobe (EMP) analysis, a non-destructive microchemical surface technique (technical details can be found in supporting information S2). Mg/Ca data provided information for temperature reconstruction and sample chronology (for data handling see supporting information S4).

The entire sample section (about 60x12 mm^2) was first analyzed by EMP in low resolution (30 µm) (see Figure 2A). Based on this overview map two sample areas (covering the last decades of 19th and 20th century; M-1887/97: 1887-1897 and M-1988/98: 1988-1998) were selected for high-resolution EMP mapping analysis (5x5 mm^2, 5 µm resolution) (Figure 2B). Within these areas the two boron images B-1888/94 and B-1989/96 have been acquired.

Further high-res EMP maps cover the areas used for the boron time series analyses TS-1923/27, TS-1961/65 and TS-1989/92 (Figure 4A), each representing at least 4-5 consecutive annual layers of undisturbed growth.

Details of the calculations used to convert $\delta^{11}B$ data into pH can be found in supporting information S4. pH is expressed as total scale. All uncertainties in the text are 1SD.

Acknowledgments .

Funding for this study was provided by the Federal Ministry of Education and Science (BMBF) joint-project BIOACID (03F0608B, TP 3.2.4) to JF, THH and FR. JH was supported by NSERC (National Science and Engineering Resource Council) and CFCAS (Canadian Foundation for Climate and Atmospheric Sciences) grants. Funding to collect specimens was provided to RSS by US National Science Foundation (grant no. PLR-1316141). Finally, the authors thank the editor and three anonymous reviewers for their constructive comments and helpful suggestions to improve the manuscript.

1. Sabine CL *et al.* (2004) The oceanic sink for anthropogenic CO_2. *Science* 305: 367-371.
2. Caldeira K, Wickett ME (2003) Oceanography: Anthropogenic carbon and ocean pH. *Nature* 425: 365-365.
3. *IPCC Climate Change 2013: The Physical Science Basis, Contribution of Working Group I to the Fifth Assessment Report of the Intergovernmental Panel on Climate Change* (2013) eds Stocker TF, Qin D, Plattner GK, Tignor M, Allen SK, Boschung J, Nauels JA, Xia Y, Bex V, Midgley PM (Cambridge Univ. Press).
4. Orr JC *et al.* (2005) Anthropogenic ocean acidification over the twenty-first century and its impact on calcifying organisms. *Nature* 437: 681-686.
5. Hofmann GE *et al.* (2010) The Effect of Ocean Acidification on calcifying organisms in marine ecosystem: an organisms-to-ecosystem Perspective. *Annu. Rev. Ecol. Evol. Syst.* 41: 127-147.
6. Kuffner IB, Andersson AJ, Jockel PL, Rodgers KS, Mackenzie FT (2008) Decreased abundance of crustose coralline algae due to ocean acidification. *Nature Geosci.* 1: 114-117.
7. Zeebe RE, Wolf-Gladrow DA (2001) CO_2 in Seawater: Equilibrium, Kinetics, Isotopes. *Elsevier Oceanography Series* 65 (Elsevier, Amsterdam), pp 346.
8. Ragazzola F *et al.* (2012) Ocean acidification weakens the structural integrity of coralline algae. *Global Change Biology* 18: 2804-2812.
9. Martin S, Gattuso JP (2009) Response of Mediterranean coralline algae to ocean acidification and elevated temperature. *Global Change Biology* 15: 2089-2100.
10. Hönisch B *et al.* (2012) The geologic record of ocean acidification. *Science* 335: 1058-1063.
11. Hemming NG, Hanson GN (1992) Boron isotopic composition and concentration in modern marine carbonates. *Geochim. Cosmochim. Acta* 56: 537-543.
12. Hönisch B, Hemming NG (2005) Surface ocean pH response to variations in pCO_2 through two full glacial cycles. *Earth Planet. Sci Lett.* 236: 305-314.
13. Kasemann SA, Schmidt DN, Bijma J, Foster GL (2009) In situ boron isotope analysis in marine carbonates and its application for formaminifera and palaeo-pH. *Chem. Geol.* 260: 138-147.
14. Foster GL, Ni Y, Haley B, Elliot T (2006) Accurate and precise isotopic measurement of sub-nanogram sized samples of foraminiferal hosted boron by total evaporation NTIMS. *Chem. Geol.* 230: 161-174.
15. Pelejero C *et al.* (2005) Preindustrial to modern interdecadal variability in coral reef pH. *Science* 309: 2204-2207.
16. Foster GL (2008) Seawater pH, pCO_2 and $[CO_3^{2-}]$ variations in the Caribbean Sea over the last 130 kyr: a boron isotope and B/Ca study of planktic foraminifera. *Earth. Planet. Sci. Lett.* 271: 254-266.
17. Douville E *et al.* (2010) Abrupt sea surface pH change at the end of the Younger Dryas in the central sub-equatorial Pacific inferred from boron isotope abundance in corals (Porites). *Biogeosci.* 7: 244/2459.
18. Fietzke J *et al.* (2010) Boron isotope ratio determination in carbonates via LA-MC-ICP-MS using soda-lime glass standards as reference material. *J. Anal. At. Spectrom.* 25: 1953-1957.
19. Halfar J *et al.* (2011) 225 years of Bering Sea climate and ecosystem dynamics revealed by coralline algal growth-increment widths. *Geology* 39: 579-582.
20. Freiwald A, Henrich R (1994) Reefal coralline algal build-ups within the Arctic Circle: morphology and sedimentary dynamics under extreme environmental seasonality. *Sedimentology* 41: 963-984.
21. Foster MS (2001) Rhodoliths: between rocks and soft places *J. Phycol.* 37: 659-667.
22. Kamenos NA, Law A (2010) Temperature controls on coralline algal skeletal growth. *J. Phycol.* 46: 331-335.
23. Digby PSB (1977) Photosynthesis and respiration in the coralline algae, Clathromorphum circumscriptum and Corallina officinalis and the metabolic basis of calcification. *J. Mar. Biol. Assoc. UK* 57: 1111-1124.
24. Halfar J, Steneck RS, Joachimski M, Kronz A, Wanamaker Jr AD (2008) Coralline red algae as high resolution climate recorders. *Geology* 36: 463-466.
25. Kamenos NA, Cusack M, Moore PG (2008) Coralline algae are global palaeothermometers with be-weekly resolution. *Geochim. Cosmochim. Acta* 72: 771-779.
26. Smith TM, Reynolds RW (2004) Improved extended reconstruction of SST (1854-1997). *J. Clim.* 17: 2466-2477.
27. Reed RK, Stabeno PJ (1994) Flow along and across the Aleutian ridge. *J. Mar. Res.* 52: 639-648.
28. Reed RK, Stabeno PJ (1999) The Aleutian North Slope Current. *Dynamics of the Bering Sea: A Summary of Physical, Chemical, and Biological Characteristics, and a Synopsis of Research on the Bering Sea,* eds Loughlin TR, Ohtani K (*PICES*), 177–191.
29. Halfar J *et al.* (2007) Coralline alga reveals first marine record of subarctic North Pacific climate change. *Geophys. Res. Lett.* 34: 5pp.
30. Adey WH (1965) The genus Clathromorphum (Corallinaceae) in the Gulf of Maine. *Hydrobiologia* 26: 539-573.
31. Halfar J, Zack T, Kronz A, Zachos JC (2000) Growth and high-resolution paleoenvironmental signals of rohodoliths (coralline red algae): a new biogenic archive. *J. Geophys. Res.* 105: 107-122.
32. Hetzinger S *et al.* (2009) High-resolution Mg/Ca ratios in a coralline red alga as a proxy for Bering Sea temperature variations from 1902 to 1967. *Palaios* 24: 406-412.
33. McCulloch M *et al.* (2012) Resilience of cold-water sclractinian corals to ocean acidification: Boron isotopic systematics of pH and saturation state up regulation. *Geochim. Cosmochim. Acta* 87: 21-34.
34. McCulloch M, Falter J, Trotter J, Montagna P (2012) Coral resilience to ocean acidification and global warming through pH up-regulation. *Nature Climate Change* 2: 623-627.
35. Krief S *et al.* (2010) Physiological and isotopic responses of scleractinian corals to ocean acidification. *Geochim. Cosmochim. Acta* 74: 4988-5001.
36. Holcomb M *et al.* (2014) Coral calcifying fluid pH dictates response to ocean acidification. *Sci Reports* 4: 5207.
37. Comeau S, Carpenter RC, Edmunds PJ. (2012) Coral reef calcifiers buffer their response to ocean acidification using both bicarbonate and carbonate. *Proc R Soc B* 280: 20122374.
38. Takahashi T *et al.* (2014) Climatological distributions of pH, pCO_2, total CO_2, alkalinity,and $CaCO_3$ saturation in the global surface ocean, and temporal changes at selected locations. *Marine Chem.* 164: 95-125.
39. Mann KH (1973) Seaweeds: Their Productivity and Strategy for Growth. *Science* 182: 975-981.
40. Wilmers CC, Estes JA, Edwards M, Laidre KL, Konar B (2012) Do trophic cascades affect the storage and flux of atmospheric carbon? An analysis of sea otter and kelp forests. *Front. Ecol. Environ.* 10: 409-415.
41. Hofmann GE *et al.* (2011) High-Frequency Dynamics of Ocean pH: A Multi-Ecosystem Comparison. *PLoS ONE* 6: e28983.
42. Doty MS, Oguri M (1956) The Island Mass Effect. *J. du Conseil, Conseil Internat. pour l'Explor. de la Mer* 22: 33– 37.
43. Caldeira RMA, Groom S, Miller P, Pilgrim D, Nezlin NP (2002) Sea-surface signatures of the island mass effect phenomena around Madeira Island, Northeast Atlantic. *Remote Sensing of Environment* 80: 336-360.
44. Hetzinger S *et al.* (2011) High-resolution analysis of trace elements in crustose coralline algae from the North Atlantic and North Pacific by laser ablation ICP-MS. *Palaeogeography, Palaeoclimatology, Palaeoecology* 302: 81-94.
45. Coplen TB (2011) Guidelines and recommended terms for expression of stable isotope-ratio and gas-ratio measurement results. *Rapid Commun. Mass Spectrom.* 25: 2538-2560.
46. Klochko K, Kaufman AJ, Yao W, Byrne RH, Tossel JA (2006) Experimental measurement of boron isotope fractionation in seawater *Earth Planet. Sci. Lett.* 248: 276-285.
47. Dickson AG (1990) Thermodynamics of the dissociation of boric-acid in synthetic seawater from 273.15-K to 318.15-K. *Deep-Sea Res.* 37: 755-766.
48. Foster GL, Pogge von Strandmann PAE, Rae JWB (2010) Boron and magnesium isotopic composition of seawater. *Geochem. Geophys. Geosyst*. 11: Q08015.